JGR Earth Surface

RESEARCH ARTICLE
10.1029/2023JF007082

Spatial Response of Greenland's Firn Layer to NAO Variability

M. Brils[1], P. Kuipers Munneke[1], and M. R. van den Broeke[1]

[1]Institute for Marine and Atmospheric Research, Utrecht University, Utrecht, The Netherlands

Key Points:

- The thickness and pore space of Greenland's firn layer respond spatially heterogeneously to changes in the North Atlantic Oscillation (NAO)
- After 2012, a more positive NAO led to thickening and cooling of the firn layer in some regions, but not everywhere
- The amplitude of the seasonal cycle in firn thickness is linked to the seasonality of the polar jet stream

Correspondence to:

M. Brils,
m.brils@uu.nl

Citation:

Brils, M., Kuipers Munneke, P., & van den Broeke, M. R. (2023). Spatial response of Greenland's firn layer to NAO variability. *Journal of Geophysical Research: Earth Surface*, *128*, e2023JF007082. https://doi.org/10.1029/2023JF007082

Received 25 JAN 2023
Accepted 20 JUL 2023

Abstract Firn on the Greenland Ice Sheet (GrIS) buffers meltwater, and has a variable thickness, complicating observations of volume change to mass change. In this study, we use a firn model (IMAU-FDM v1.2G) forced by a regional climate model (RACMO2.3p2) to investigate how the GrIS firn layer thickness and pore space have evolved since 1958 in response to variability in the large-scale atmospheric circulation. On interannual timescales, the firn layer thickness and pore space show a spatially heterogeneous response to variability in the North Atlantic Oscillation (NAO). Notably, a stronger NAO following the record warm summer of 2012 led the firn layer in the south and east of the ice sheet to regain thickness and pore space after a period of thinning and reduced pore space. In the southwest, a decrease in melt dominated after 2012, whereas in the east, the main driver was an increase in snow accumulation. At the same time, the firn in the northwestern ice sheet continued to lose pore space. The NAO also varies on intra-annual timescales, being typically stronger in winter than in summer. This impacts the amplitude of the seasonal cycle in GrIS firn thickness and pore space. In the wet southeastern GrIS, most of the snow accumulates during the winter, when melting and densification are relatively weak, leading to a large seasonal cycle in thickness and pore space. The opposite occurs in other regions, where snowfall peaks in summer or autumn. This dampens the seasonal amplitude of firn thickness and pore space.

Plain Language Summary Most of the Greenland ice sheet's surface is covered by a layer of firn, which is compressed snow that can retain meltwater within its pores, and in this way buffer runoff into the ocean. Loss of pore space thus amplifies future Greenland ice-sheet mass loss and accelerates sea-level rise. We use computer models of the firn layer to investigate how firn has evolved from 1958 to 2020. The firn layer has gotten substantially thinner, less porous, and warmer over this period, but the changes are not the same everywhere. Moreover, after 2012, the firn in some regions recovered some of its lost pore space. These changes are linked to changes in the jet stream, a band of strong westerly winds encircling the Northern Hemisphere. A weaker and more meandering jet stream enhances the loss of pore space and vice versa. The jet stream also impacts the seasonal distribution of snowfall, and in this way, it influences the seasonal cycle of the firn depth and pore space.

1. Introduction

Since the 1990s, the Greenland ice sheet (GrIS) has been losing mass at an increasing rate (Shepherd et al., 2020), contributing to the observed, persistent acceleration in global mean sea-level rise (Dangendorf et al., 2019). About half of the recent GrIS mass loss is caused by faster ice flow and subsequent calving of icebergs, the other half is due to increased surface melt and subsequent runoff (Enderlin et al., 2014; Mouginot et al., 2019). The runoff increase would have been greater were it not for the porous firn layer that covers ~90% of the ice sheet. An estimated 45% of all surface meltwater refreezes in the firn (Van den Broeke et al., 2016) or is retained in perennial aquifers (Forster et al., 2014). For Greenland's glaciers and ice caps disconnected from the main ice sheet, the buffering effect that refreezing has on runoff has deteriorated since the mid 1990s (B. Noël et al., 2017). Consequently, their mass loss accelerated (Khan et al., 2022). In the future, large areas of the contiguous GrIS may also become affected by reduced firn pore space (also called firn air content, FAC hereafter) leading to less efficient refreezing and accelerated mass loss (B. Noël et al., 2021).

Apart from having a direct impact on ice-sheet mass balance through meltwater retention, the firn layer also impacts the observation of contemporary GrIS mass loss. A common method to assess GrIS mass balance is altimetry (Khan et al., 2022). With altimetry, the ice-sheet surface is repeatedly scanned with laser or radar instruments onboard planes or satellites (Sandberg Sørensen et al., 2018). In this way, surface elevation change is

measured and thus, under certain assumptions, volume change. To convert volume to mass change, knowledge of the density associated with the observed elevation change is required (McMillan et al., 2016). This complicates the conversion since the thickness and density of the firn layer is not uniform and may change through for example, variability in snowfall, firn compaction and meltwater refreezing. The latter two processes change the firn air content (FAC) of the firn layer (and hence the surface elevation) but not its mass.

To understand the past, present, and future contribution of the GrIS to sea-level rise, we thus need to understand how the firn layer's thickness, density and temperature has responded and will respond to changes in the climate. Firn thickness, density and temperature are determined mainly by weather and climate conditions at the surface, notably variations in snow accumulation, liquid water input from melt or rain, and surface temperature. Large-scale circulation variability dictates variations in atmospheric temperature, melt and snowfall. For example, Greenland blocking constitutes a less zonally oriented polar jet stream and a negative North Atlantic Oscillation (NAO) index (Bevis et al., 2019; Hanna et al., 2022; Huai et al., 2020). An increased frequency of Greenland blocking episodes led to multiple strong summer melting events since the beginning of the 2000s (McLeod & Mote, 2016; Zhang et al., 2019). Recent observations show increased firn temperatures across the GrIS (McGrath et al., 2013; Orsi et al., 2017; Polashenski et al., 2014) in response to significant Greenland atmospheric warming (Hanna et al., 2013). Higher atmospheric and surface temperatures lead to an increase in melt, latent heat release upon refreezing, stronger firn densification and thus a loss of FAC. At the same time, firn cores drilled in southwest Greenland reveal that FAC recently increased following several colder summers (Rennermalm et al., 2022), implying that the near-surface firn can also recover relatively quickly.

Unfortunately, in situ firn measurements are scarce and have limited temporal resolution. This makes it harder to generalize the findings based on such observations and to determine the large-scale drivers of the observed changes in the firn layer. A firn model, forced at its upper boundary by a climate model, is a useful tool to disentangle elevation changes caused by mass and non-mass conserving processes (Hawley et al., 2020; Zwally & Jun 2002). Moreover, it can do so over the full GrIS and on inter- and intra-annual (seasonal) time scales, including the effect of large-scale atmospheric variability. While the effect of the polar jet stream on the atmospheric circulation over the GrIS and its surface mass balance (SMB) has been reported before (Ramos Buarque & Salas y Melia, 2018), there has not been a study that directly links changes in the large-scale circulation to changes in the firn layer. In this study, we use the firn model IMAU-FDM v1.2G, forced by the polar regional climate model RACMOv2.3p2 (Brils et al., 2021), to investigate the role of recent large-scale circulation variability on firn thickness and air content. We first discuss GrIS integrated changes and how they contrast at high and low ice-sheet elevations (Section 3.1). In Section 3.2, we partition the ice sheet into multiple sections and find very different regional responses. Section 4 couples these patterns to large-scale atmospheric circulation variability, notably the NAO. By separating intra-annual (seasonal) from interannual variability, we demonstrate how the NAO plays an important role on both time scales. Our conclusions are summarized in Section 5.

2. Methods

2.1. IMAU-FDM

Firn models are often employed to provide information on the characteristics of the firn layer over the GrIS, usually covering the period after 1958, that has sufficiently reliable atmospheric reanalyses for the Northern Hemisphere. Such stand-alone firn models have several advantages compared to regional climate models that include a firn model. They typically have a higher vertical resolution, which is necessary to resolve the heterogeneous density and water content of the firn layer. Moreover, they allow for a more detailed representation of the physical processes that govern firn densification (Stevens et al., 2020). Dedicated firn models are also much cheaper to run than regional climate models. This enables performing numerous sensitivity tests to calibrate and evaluate their performance (Brils et al., 2021; Kuipers Munneke et al., 2015; Ligtenberg et al., 2011). As a final advantage, the computational efficiency allows stand-alone firn models to be initialized to a proper equilibrium state. An obvious disadvantage is the lack of two-way coupling between the firn layer and the atmosphere.

In this study, we use a dedicated firn model, IMAU-FDM version 1.2G. Details of IMAU-FDM parametrizations and evaluation for the GrIS can be found in Brils et al. (2021). Here, we will briefly discuss its main characteristics. IMAU-FDM is a one-dimensional model with a Lagrangian description of the firn. This means that its grid cells follow the same parcel of mass over time, which is advected downwards or upwards whenever the firn

thickness increases or decreases. In this framework, the equation that describes the densification rate of the firn is simplified to a semi-empirical equation without the need to explicitly calculate the vertical advection terms (Herron & Langway, 1980). Since there exists a correlation between the mean accumulation rate and the densification rate on the GrIS and Antarctic ice sheet, the inclusion of an accumulation-dependent prefactor leads to an improved performance (Kuipers Munneke et al., 2015; Ligtenberg et al., 2011). This factor was recalibrated in v1.2G of IMAU-FDM, further improving the performance for the GrIS (Brils et al., 2021). In addition to the densification equation, the model implicitly solves the 1D heat equation via the Crank-Nicolson scheme (Crank & Nicolson, 1947) and includes latent heat release by refreezing liquid water. The firn's simulated temperature has been evaluated against in situ measurements showing a root-mean-square error (RMSE) of 3.1°C, caused by a systematic warm bias in the dry interior and a cold bias at low and wet locations (Brils et al., 2021).

Liquid water percolation through the firn is solved via a "bucket scheme." In this scheme, water percolates downward until it reaches a cold layer where it can refreeze or remain within the firn as irreducible water content. If the water cannot refreeze or be retained within the firn, it is assumed to runoff instantly. The advantage of this method is its simplicity and computational efficiency. The disadvantage is that it does not allow for standing water to occur, nor for the formation of impermeable ice layers. Nevertheless, the modeled percolation depth of meltwater is comparable to the few available measurements (Brils et al., 2021; Heilig et al., 2018). IMAU-FDM's performance in simulating liquid water content is also comparable to other models with a more elaborate handling of water percolation (Vandecrux, Mottram, et al., 2020). The model is initialized via a spin-up procedure in which it is forced with the climate of a reference period. This is repeated until the firn layer reaches a steady state, that is, the firn layer's properties do not change anymore after forcing it with the reference period. Here, the period 1960–1980 was selected because it does not exhibit strong climate trends (van Angelen et al., 2014). The firn model runs at the same horizontal resolution as its atmospheric forcing, namely 5.5 km. In the vertical, the amount of grid cells and their thickness is variable, increasing from about 3 cm near the surface to 9 cm at a depth of 100 m. The number of layers generally varies between 300 and 3,000, depending on the thickness of the firn pack. The temporal resolution is 15 min.

2.2. RACMO

At the top of the firn layer, mass may accumulate through solid precipitation, drifting snow deposition or riming, or be removed by drifting snow erosion, sublimation, and melt. Here, we define accumulation as the sum of snowfall and drifting snow deposition minus sublimation. The surface temperature, which is determined by the surface energy balance, cools or warms the firn through molecular conduction. These surface mass and heat fluxes are prescribed from three-hourly output of RACMO2.3p2, a regional atmospheric climate model that has been adapted to realistically simulate ice-sheet climates through a dedicated snow/ice albedo scheme (Kuipers Munneke et al., 2011) and the inclusion of drifting snow physics (Lenaerts et al., 2014). Bare ice albedo in the GrIS ablation zone is prescribed from MODIS observations. Previous studies have thoroughly evaluated the performance of RACMO2.3p2 over the GrIS and show satisfactory performance for both the surface mass and energy balance (Lenaerts et al., 2014; B. Noël et al., 2018; van Angelen et al., 2014). At its lateral and upper boundaries, RACMO2.3p2 is forced with data from ECMWF reanalysis data: ERA40 (Uppala et al., 2005) for the period 1 November 1957–31 December 1978, ERA-Interim (Dee et al., 2011) for the period 1979–1990 and ERA5 afterward (Hersbach et al., 2020). The 3-hourly RACMO2.3p2 output is linearly interpolated to time steps of 15 min to force the offline firn model.

3. Firn Evolution

3.1. Mean Ice-Sheet Wide Trends

A general picture of the past and current state of the GrIS firn layer can be obtained by looking at its mean thickness, its air content, and the temperature at 10 m depth. Since we focus on changes in the firn layer, we need to filter out areas of bare ice. We approximate the bare ice extent as the area with a mean negative SMB during the spin-up period (see Figure 1). This is approximately 8% of the extent of the whole ice sheet. Although by doing so, we may under- or overestimate the exact extent in certain years, for simplicity we assume this mask to be constant in time.

Figure 2a shows the evolution of the mean firn thickness averaged over the contiguous ice sheet and averaged separately for the areas below and above 2,500 m a.s.l. (Figure 1). Between 1958 and 1990, firn thickness showed

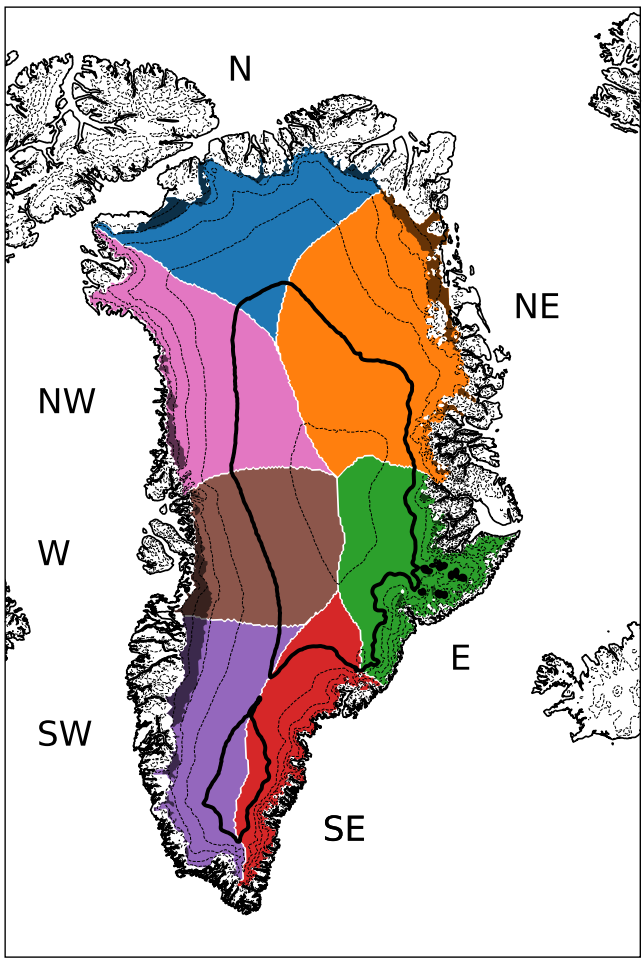

Figure 1. Map of Greenland, with colors indicating seven selected basins of the contiguous ice sheet (Greenland Ice Sheet) (taken from Mouginot et al. (2019)). Basin colors correspond to the line colors used in Figure 3. The ablation zone mask is indicated with a darker shade. The thin dashed lines represent elevation contours with an interval of 500 m and the thick solid black line indicates the 2,500 m.a.s.l. elevation contour.

consistent behavior at all elevations, with a decrease of ~1 m until the early 1970s and a relatively steady increase of similar magnitude afterward. After approximately 1990, the annual mean firn thickness started to decline. First this happened slowly, but after the early 2000s the rate increased. Between 1990 and 2005, the decline was 0.8 ± 0.1 cm/yr, but between 2005 and 2012 it increased to 15.2 ± 0.4 cm/yr. The red shaded range in the panels of Figure 2 indicates the mean value ±2 standard deviations of the variable during the spin-up period (1960–1980). Since the modeled firn layer is in equilibrium with its spin-up period, this allows us to quantify when these variables exceed the range of their natural variability. The firn thickness (Figure 2a) has exceeded this range since 2011. The high melt years 2007, 2010, 2012, and 2019 (Cullather et al., 2020; Nghiem et al., 2012) had a pronounced impact on the mean firn thickness. In between and after these high melt years, however, the firn thickness remained relatively constant. From 2013 up to and including 2020, the mean trend was modestly negative at −3.6 ± 0.4 cm/yr. The thinning of the firn layer can be fully attributed to elevations below 2,500 m a.s.l. (green line). In fact, firn thickness has increased at higher elevations, although not enough to compensate for the thinning at lower elevations.

The firn air content (FAC, Figure 2b) represents the total vertically integrated porosity of the firn column, that is, the vertical distance the firn layer can be compressed before reaching the density of ice. The theoretical maximum amount of liquid water that can be retained within the firn layer is closely related to this quantity. Therefore, trends in the FAC reflect changes in the firn's capacity to absorb meltwater. The trends in the FAC are similar to the trends in its thickness: overall the ice-sheet average FAC (red line) has been decreasing since the 1990s, with the decrease accelerating in the mid 2000s and then decelerating after 2012. Since 2011, FAC has exceeded the lower limit of variability during the period 1960–1980. Most of the FAC loss occurred below 2,500 m a.s.l. (green line), while the mean FAC remained constant in the higher interior (blue line). As a result, the gradient of FAC with elevation increased.

Temperature influences many processes in the firn layer, such as its densification rate and the amount and depth of meltwater refreezing. In the absence of melt, the temperature at 10 m depth (T_{10m}) is usually a good approximation

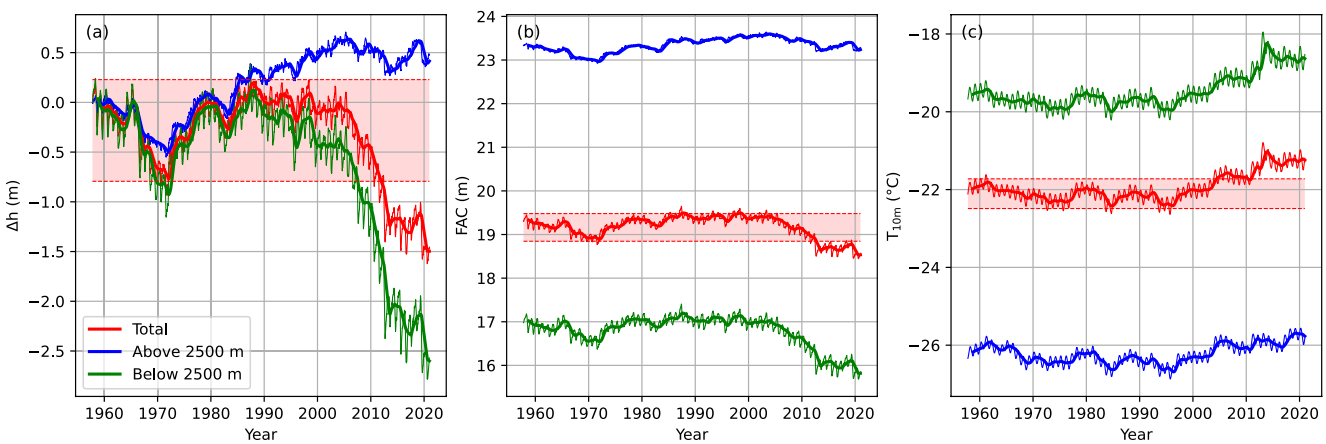

Figure 2. Time series of firn thickness changes relative to 1 November 1957 (a), firn air content (b), and T_{10m} (c) averaged for the total Greenland Ice Sheet (red), above 2,500 m (blue) and below 2,500 m (green). Bold lines indicate a running mean of 1 year. The red shaded area indicates the mean value ±2 standard deviations during spin-up.

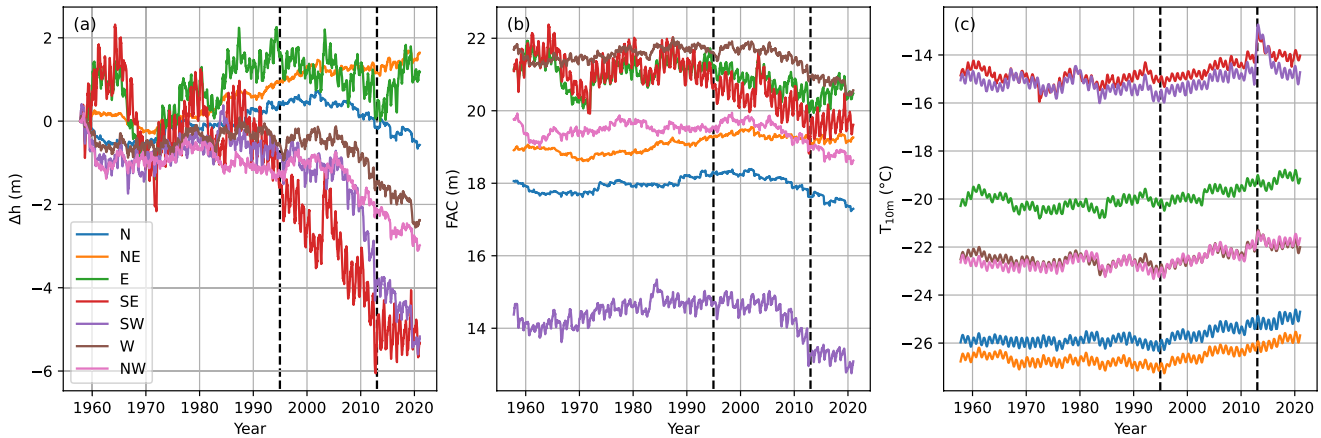

Figure 3. Time series of firn thickness changes relative to 1 November 1957 (a), firn air content (b), and T_{10m} (c), partitioned per basin as defined in Figure 1. Dashed vertical lines indicate the start of the two periods analyzed in more detail: 1995 and 2013.

of the annual mean surface temperature; below this depth, the firn is isolated from most of the seasonal cycle in surface temperature, but not completely: a small, ∼1°C seasonal oscillation remains at this depth (Figure 2c) (Cuffey & Paterson, 2011). The average surface temperature is somewhat lower than the 2 m air temperatures because of the semi-permanent surface-based temperature inversion over ice sheets in the non-summer seasons (Ettema et al., 2010). After melt occurs, the release of latent heat upon refreezing of meltwater may raise firn temperatures substantially, increasing T_{10m} beyond the surface temperature by a magnitude that depends on the amount and depth of refreezing. As such, T_{10m} can also be an indicator of warming of the firn by refreezing (Steffen & Box, 2001). For these reasons, T_{10m} is a commonly used and measured quantity. Here, we investigate its evolution.

The ice-sheet averaged T_{10m} has remained fairly constant until the mid 1990s, after which it started to increase gradually (Figure 2c, red line). In contrast to the mean firn thickness and FAC, T_{10m} increases at all elevations. However, this increase is larger at lower elevations (green line) than at higher elevations (blue line). It has also continued until the end of the period. At elevations below 2,500 m a.s.l., a clear peak in T_{10m} is modeled in 2012. Such a peak is absent at higher elevations. The T_{10m} peak at lower elevations is caused by an increase in refreezing of percolating meltwater, whereas refreezing at higher elevations, if present, occurred in smaller quantities and at shallower depths. Figure 2c also shows that the summer of 2019 had a smaller impact on the mean T_{10m} than the summer of 2012. The difference between the winter minimum and summer maximum in T_{10m} was 0.75 and 0.38°C for 2012 and 2019, respectively. Since around 2011, T_{10m} exceeds the upper bound of its natural variability during the period 1960–1980.

Since around 2011, the modeled values of FAC, firn thickness and temperature all exceed the limits of natural variability as inferred from the spin-up period (Figure 2). It indicates that, although the natural variability in the properties of the firn layer is substantial, the firn changes since the mid-1990s have emerged from the background noise and can therefore be ascribed to long-term changes in the climate.

3.2. Regional Trends

In Section 3.1, we looked at changes in firn properties, spatially integrated over the entire ice sheet. However, firn across the ice sheet is formed under different climate conditions, and so we expect that regional trends may be different from the mean. Therefore, we compare the trends within seven ice-sheet drainage basins, as defined by Mouginot et al. (2019), seeFigure 1). Figures 3a and 3b clearly show that the changes in firn thickness and FAC do not only differ between low and high elevations (Figure 2) but also vary from basin to basin. Basin NE has been thickening monotonically and gained FAC. All the other basins have experienced periods of decline in thickness and FAC during the past decades. However, the timing and rate of this loss vary. For example, the basins in the south (SW and SE) have undergone the greatest decline in FAC. The moment at which they started to decline, however, is not the same: it started in the early 1990s for the SE basin but in the mid 2000s for the SW basin. Firn thickness in the E, N, NW, and W basins also started to decrease in the early 2000s. After 2012, however, a break

Table 1
Mean Rate of Change in h, Firn Air Content and T_{10m} in Each Basin for the Periods 1995–2012 and 2013–2020

	$\frac{\partial}{\partial t}h$ (cm yr^{-1})		$\frac{\partial}{\partial t}$FAC (cm yr^{-1})		$\frac{\partial}{\partial t}T_{10m}$ (°C decade^{-1})	
Basin	1995–2012	2013–2020	1995–2012	2013–2020	1995–2012	2013–2020
N	−2.51 ± 0.09	**−5.38 ± 0.28**	−2.92 ± 0.07	**−4.41 ± 0.20**	0.41 ± 0.01	0.46 ± 0.05
NE	1.34 ± 0.07	**5.08 ± 0.24**	−0.90 ± 0.06	**1.14 ± 0.18**	0.43 ± 0.01	**0.58 ± 0.04**
E	−3.79 ± 0.23	**15.24 ± 0.75**	−4.06 ± 0.16	**5.93 ± 0.54**	0.49 ± 0.01	**0.53 ± 0.05**
SE	−16.48 ± 0.43	**−2.16 ± 0.89**	−5.15 ± 0.28	**2.08 ± 0.64**	0.59 ± 0.01	**−0.96 ± 0.05**
SW	−12.14 ± 0.37	**−19.51 ± 0.59**	−5.33 ± 0.22	**−4.30 ± 0.40**	0.65 ± 0.02	**−2.44 ± 0.08**
W	−3.76 ± 0.18	**−11.51 ± 0.38**	−2.97 ± 0.12	**−5.33 ± 0.26**	0.50 ± 0.01	**−0.50 ± 0.05**
NW	−5.76 ± 0.19	**−9.56 ± 0.37**	−3.48 ± 0.11	**−4.08 ± 0.25**	0.47 ± 0.02	**−0.14 ± 0.04**

Note. If the 2013–2020 trend is significantly different ($p < 0.05$) from the 1995–2012 trend, it is written in boldface.

in these trends occurred for many basins, and firn started to thicken again in the NE, SE, and E basins and decline at a slower pace in the SW. Similar trends are observed for the FAC (Figure 3b).

Confirming the ice-sheet wide picture discussed in Section 3.1, T_{10m} has been rising in all the basins since the 1990s. However, in the SW and SE basins, and to a lesser extent in W and NW, we observe a peak in T_{10m} occurring in the summer of 2012, which is absent in the other basins. After this peak, the firn's temperature remained steady or slowly declined over time, whereas in the other basins it kept rising. We also note that no clear peak can be distinguished in the summer of 2019 in any of the basins. This suggests that percolation and refreezing were able to affect temperature at a depth of 10 m or more only in 2012 and in these southern and western basins, even though enhanced surface melt occurred in all basins (Tedesco & Fettweis, 2020).

The amplitude of the seasonal cycle in firn thickness and FAC varies greatly per basin. In general, the eastern basins show a greater seasonal amplitude than their western counterparts. Moreover, the basins in the north show very little seasonal variations in thickness and FAC. For T_{10m}, these differences between basins are not observed and the seasonality is roughly the same everywhere.

We performed a linear regression for each basin to determine the mean rate of change in firn thickness, FAC and T_{10m} during the periods 1995–2012 and 2013–2020. These periods correspond to periods with a predominantly negative and positive NAO phase, respectively (Figure 5c). This will be discussed in more detail in Section 4.1. The rates are summarized in Table 1. The similarity between the trends in firn thickness and FAC is apparent. The break in many trendlines in 2012 shows up as a change in the sign of the rate of change. In order to determine whether the pre- and post 2012 trends are significantly different, we performed a Chow test. It shows that all trends have changed significantly in 2012 ($p < 0.05$), except for the trends of T_{10m} in the N basin. Note that the trendline in the SW basin does not reflect the slowdown in thinning mentioned earlier. This is a consequence of letting the first period start in 1995, whereas the thinning of firn in the SW mostly accelerated since 2005. The linear trend of the SW basin's firn thickness for the period 2005–2012 is −36.0 ± 0.8 cm yr^{-1}, that is, thinning significantly faster than after 2012.

4. Atmospheric Drivers

4.1. Interannual Variability

The observed changes in firn properties in recent decades are caused by trends and variability in the atmospheric forcing at the ice-sheet surface. The fact that there exist very different responses across different regions (Figures 2 and 3) suggests that the atmospheric conditions over the ice sheet also varied. Figure 4 summarizes the cascade of processes through which large-scale atmospheric circulation impacts the properties of the firn layer in the absence of melt. For instance, an increase in atmospheric temperature generally leads to an increase in surface temperature by increasing downwelling longwave radiation and sensible heat fluxes, which warms the firn through molecular conduction (De La Peña et al., 2015; Hanna et al., 2021). Since firn densification is a thermally activated process, an increase in its temperature also leads to a faster compaction (Jun & Zwally, 2002;

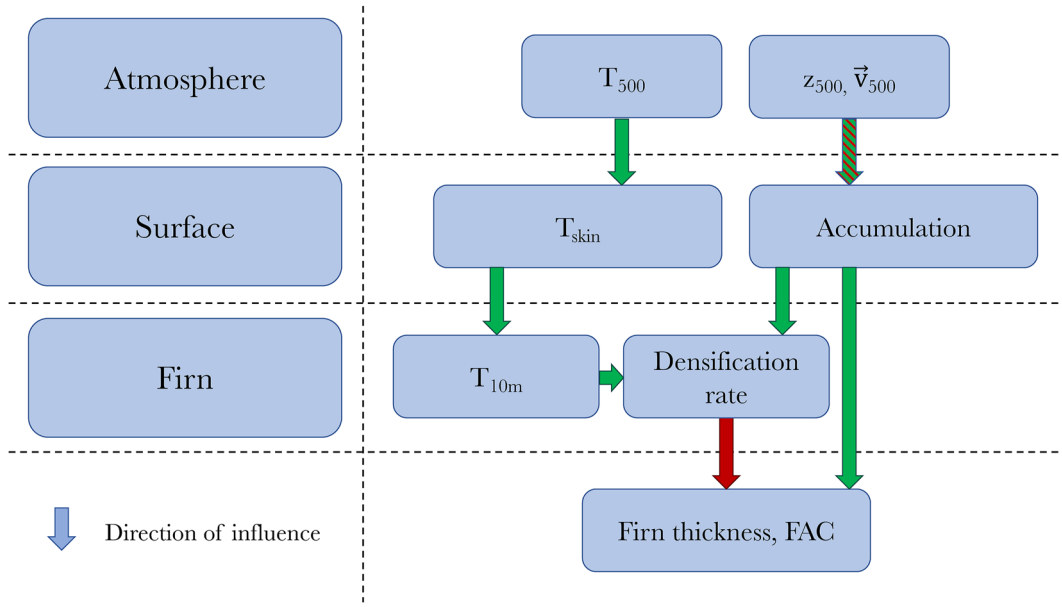

Figure 4. Schematic showing how variables in the atmosphere, at the surface and at depth in the firn influence the thickness, air content and temperature of the firn, in the absence of melt. The color of an arrow is green when the feedback is positive, red if negative, and hashed in red and green if both are possible.

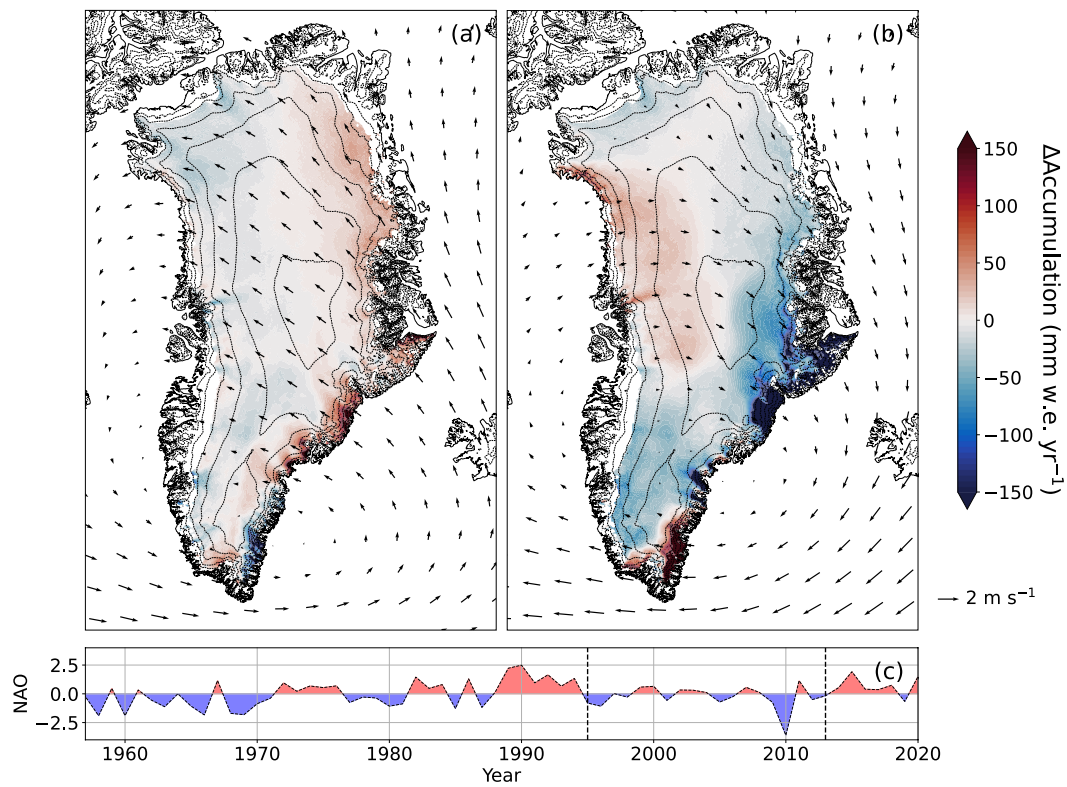

Figure 5. Mean difference in the annual Greenland Ice Sheet snow accumulation (in mm w.e. per year) and 500 hPa winds between a positive North Atlantic Oscillation (NAO) index and neutral NAO index (a) and between a negative NAO index and neutral NAO index (b). Mean patterns are calculated by averaging the wind components and mean annual accumulation rate of all years in our simulation period (1958–2020) that coincide with a positive, neutral or negative NAO index. Then, the mean positive/negative NAO patterns are subtracted from the neutral NAO pattern. The evolution of the annual NAO index is shown in panel (c) Dashed vertical lines indicate the start of the two periods analyzed in more detail: 1995 and 2013.

Herron & Langway, 1980). More snow accumulation leads on one hand to increased firn thickness, but also to enhanced densification through increased overburden pressure. Enhanced densification in turn decreases the thickness and air content of the firn column (Zwally & Jun 2002).

The amount of accumulation, melt and heating or cooling at the firn layer's surface is governed in large part by the atmospheric circulation above the GrIS. The mean large-scale circulation at 500 hPa over the ice sheet (arrows in Figures 5a and 5b) varies with the strength and zonality of the jet-stream. The strength of the jet stream over Greenland is strongly correlated with the NAO index (Hall et al., 2015). The NAO index is usually defined as the normalized sea-level pressure difference between Iceland and the Azores, its mean equaling 0.0 and its standard deviation 1.0 (Hurrell & Deser, 2009). High values of the NAO index coincide with a strong and zonal jet stream, and low NAO index with a weak and more meridionally oriented jet stream. Here, we use the annual NAO index by Hurrell et al. (2003). This index is computed as the leading EOF of the annual mean sea-level pressure over the Atlantic sector based on reanalysis data from NCAR. In this paper, we refer to the NAO index as neutral if it falls within±one third of its standard deviation, positive when it is higher than one third of its standard deviation and negative when it is lower than minus one third of its standard deviation.

A positive NAO phase leads to more zonal flow south of Greenland and a deeper Icelandic Low to the south-east of Greenland (The Icelandic Low is a semi-permanent, climatological low-pressure area typically located between Iceland and Greenland). Consequently, 500 hPa winds over the ice sheet have a more southeasterly component (Figure 5a). A negative NAO index represents a weaker Icelandic Low, and thus a more southerly and westerly component in ice-sheet 500 hPa winds at higher latitudes. As a result, positive and negative NAO states yield very different accumulation patterns (colors in Figure 5). A positive NAO index (Figure 5a) results in higher-than-average accumulation along Greenland's east coast, and negative anomalies in the interior and western parts. The divide between positive and negative accumulation anomalies follows the continental divide in elevation. However, a negative NAO index (Figure 5b) gives negative accumulation anomalies along the east coast, apart from the far southeast where the circulation anomaly has an onshore component leading to more precipitation. This opposing pattern between east and west Greenland explains why the distribution of accumulation is influenced by the NAO index, while its total sum does not correlate significantly with it (Hanna et al., 2011). Note, however, that the positive and negative NAO index accumulation patterns are not exactly each other's opposite. The patterns in Figure 5 are the mean of multiple years. The actual pattern during a single year varies from this as the exact position and strength of the jet stream also differs from year to year. This is represented in the NAO index (Figure 5c). Recall that the NAO index has a variance of unity.

The occurrence of melt complicates the schematic in Figure 4. It decreases the thickness and air content through the removal of low-density firn at the surface. Refreezing locally increases the firn density and temperature through the release of latent heat. Above 2,500 m a.s.l., however, the amount of melt is more than an order of magnitude smaller than the amount of accumulation (272 mm w.e. per year of accumulation vs. 8 mm w.e. per year melt, on average). Therefore, in these regions, changes in depth of the firn layer are often dominated by changes in accumulation.

In Section 3, we showed that, between the 1990s and 2012, the simulated thickness and FAC of the firn layer decreased everywhere, except at higher elevations. Most notably in the NE basin, there has been an overall thickening of the firn. Simultaneously, $T_{10\mathrm{m}}$ increased. Then after 2012, the rate at which the thickness and FAC decreased, decelerated in most regions. In the eastern and southern basins, the thickness and FAC even started to increase. On the other hand, in the northwest GrIS, the decrease accelerated. The temperature of the firn in the south of the GrIS also peaked in 2012 and started to decrease afterward.

To interpret these results, we discuss the modeled firn behavior before and after 2012 in the context of changes in atmospheric circulation, accumulation, and atmospheric temperature (Figures 6a and 6b). In general, while the period 1995–2012 saw a predominantly negative NAO index (Fettweis et al., 2013; Hanna et al., 2015), after 2012 the NAO index returned to a more positive value (Hanna et al., 2022). The annual mean NAO index increased from -0.0 ± 0.4 during 1995–2012 to 0.2 ± 0.3 during 2013–2020 (Figure 5c). This shift toward a more positive annual NAO index occurred mostly in winter: the winter NAO index changed from 0 ± 1 to 0.7 (± 0.5), whereas the mean summer NAO index barely changed (from -0.1 ± 0.3 to -0.1 ± 0.5). This shift resulted in, on average, a lower geopotential height of the 500 hPa plane (z_{500}) near the southern tip of Greenland and higher $z500$ toward the northeast of Greenland (Figure 6a). Consequently, the large-scale atmospheric circulation obtained an anomalous component from the east. Over the southern part of the GrIS, this easterly wind anomaly also has a small northerly component, whereas for the rest of the ice sheet, the wind anomaly has a southerly component.

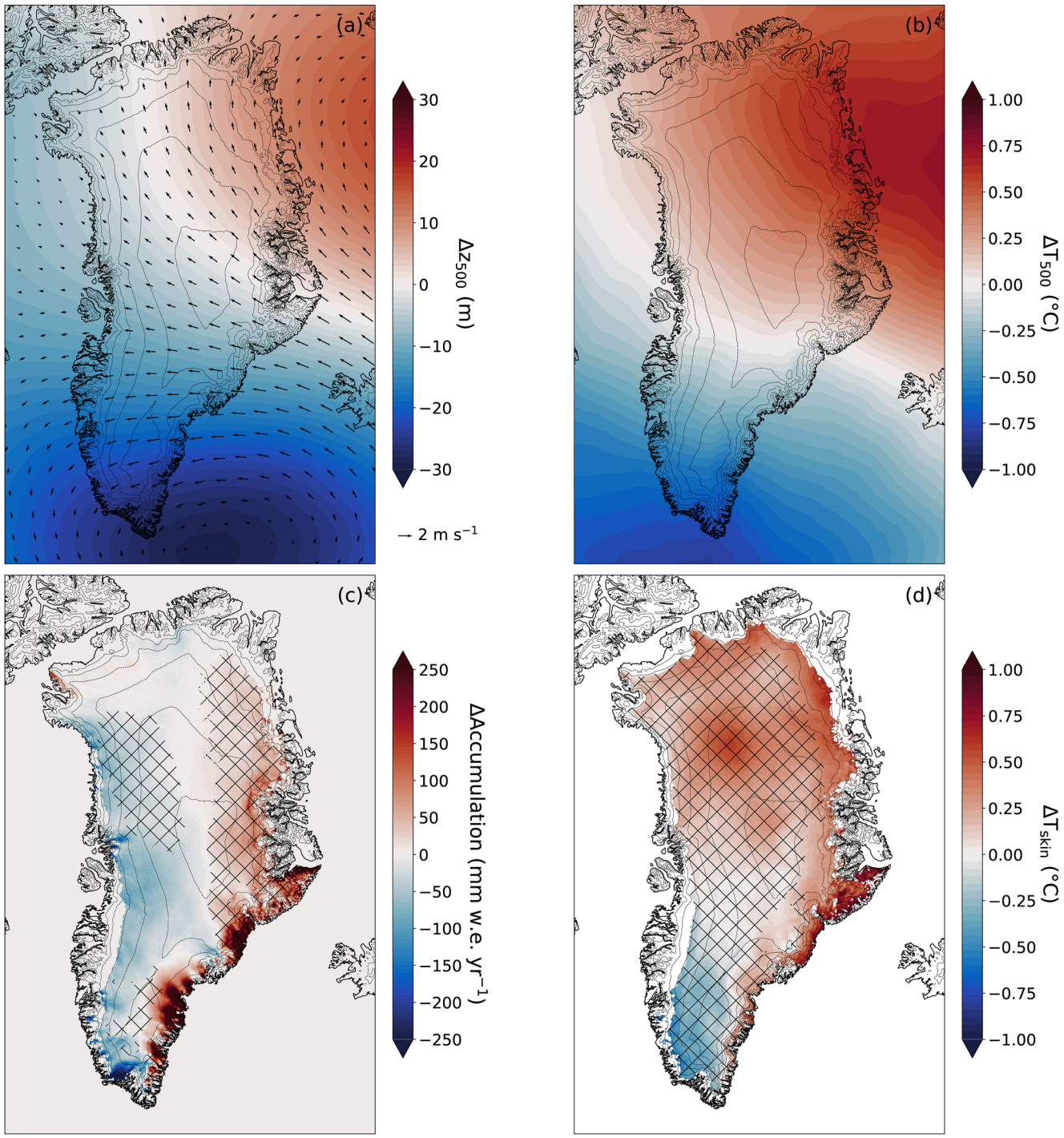

Figure 6. Difference in atmospheric and surface conditions between the periods 1995–2012 and 2013–2020. (a) Mean difference in the geopotential height of the 500 hPa pressure-level (2013–2020 minus 1995–2012). Arrows indicate the difference vector of the mean wind at 500 hPa. (b) Mean difference in the temperature at 500 hPa. (c) Mean difference in the accumulation rate. (d) Mean difference in skin temperature. In (c and d), regions where the accumulation rate and skin temperature correlate significantly with the North Atlantic Oscillation index ($p < 0.05$) are hatched. Hatching is not applied to (a and b).

Southerly winds generally bring warm air from lower latitudes and consequently, the temperature at 500 hPa (T_{500}) further increased in the north and decreased in the south of the GrIS after 2012 (Figure 6b).

The changing patterns of wind and temperature in the free atmosphere translate to accumulation and surface temperature changes (Figures 6c and 6d). There is a clear east-west gradient in accumulation because of the shift

to a more easterly circulation after 2012. This pattern in precipitation closely follows the topography of the ice sheet. The pattern closely resembles that of Figure 5a, but not exactly, which demonstrates the internal variability in the position of the jet stream and individual cyclonic events. Changes in surface temperature (Figure 6d) are very similar to the temperature pattern at 500 hPa. A strong north-south gradient in the surface temperature is observed, with strongest warming in the central and northern parts of the GrIS, and cooling in the south. The area that experienced cooling does not, however, extend as far north as the positive atmospheric temperature anomalies at 500 hPa. This is due to an increase in cloud cover over the southeastern part of the ice sheet (not shown), and consequently an increase in downwelling longwave radiation over this region. Although the net radiative effect of clouds over the GrIS is an active area of research, high albedo surfaces such as the GrIS's accumulation zone are relatively insensitive to changes in shortwave radiation, and in the radiative cloud effect longwave warming dominates over shortwave cooling in this part of the ice sheet (Wang et al., 2018, 2019). Overall, the GrIS-wide mean correlation between the annual mean T_{10m} and T_{skin} is 0.31. This is lower than the correlation of 0.80 between T_{skin} and T_{500}, reflecting the nonlinear effect that latent heat release by refreezing has on firn temperatures.

After 2012, the SW basin experienced substantial deceleration of FAC loss, and the SE basin even saw an increase in FAC (Figure 3). However, the main drivers for these changes differ between the basins. In the case of the SW basin, it is mostly driven by lower temperatures and, consequently, less melt and lower compaction rates. However, for the SE basin, the change is not dominated by a decrease in melt but by an increase in snow accumulation. Melt and compaction combined decreased by 12% in the SW but increased by 2% in the SE. Accumulation decreased by 8% in the SW and increased by 9% in the SE. Accumulation also drives the different trends at higher latitudes, where melt occurs less frequently. The E and NE basins increase in FAC whereas in the W and NW basins the FAC has decreased. This follows the east-west gradient in accumulation.

The two periods before and after 2012 span multiple years but have different lengths. Multidecadal variability might also play a role at these timescales. The main mode of multidecadal atmospheric variability in Greenland is the Atlantic multidecadal oscillation (AMO). It is known that the AMO correlates with runoff from the GrIS (Hanna et al., 2011). Both periods are, however, much shorter than the AMO period, which is typically 30–40 years, and both periods fall in a predominately positive AMO phase. Therefore, the influence of the AMO on the firn layer is similar in both periods. Moreover, the AMO is anticorrelated with the summer NAO (Folland et al., 2009). As mentioned earlier, the summer NAO changed little after 2012.

In the previous paragraphs, we restricted our analysis to comparing the periods preceding and following the high melt year of 2012. This allowed us to understand what caused the trend change in the firn thickness, FAC and T_{10m}, summarized in Table 1. It demonstrates how the firn layer evolves differently during a period with a predominantly negative NAO index compared to a period with a predominantly positive one. In order to generalize these findings to arbitrary changes in the NAO index, we use linear regression to determine how the rate of change of each variable changes with the NAO index (Figure 7). For firn thickness, an increase in the NAO leads to a larger thickening rate/slower thinning rate in the eastern and southern parts of the GrIS, and the opposite in the northwest. A very similar sensitivity is observed for FAC. The patterns closely resemble the pattern of the accumulation rate anomaly under positive NAO conditions (Figure 5a). In addition, the areas where the sensitivities are statistically significant also largely coincide with the area where the accumulation rate correlates significantly with the NAO (Figure 6c), illustrating that accumulation is the main process through which the NAO exerts its influence on the firn for most of the ice sheet. On average, T_{10m} cools faster/warms slower when the NAO is more positive. This is the case for the entire ice sheet, but the effect is strongest near the margins and statistically more significant in the south. This shows the large impact that the release of latent heat during refreezing of meltwater has on the firn's temperature. A more positive NAO leads to less blocking events and thus less melt, especially in the south (Hanna et al., 2013). As the hatching in Figure 6d shows, the firn's skin temperatures also correlate significantly with the NAO.

Our results show that care should be taken when trends observed by in situ measurements are extrapolated to larger regions, as a change in the NAO does not lead to a spatially uniform response in Greenland's firn layer. For example, Rennermalm et al. (2022) observed that the pore space of the firn in the southwest of the GrIS has increased after 2012. Here, we show that this coincided with a decrease in pore space in the northwest. Care also must be taken when extrapolating observations into the future since the NAO is highly variable. We see that the warming in the northeast between 1982 and 2011 as observed by Orsi et al. (2017) has continued in those regions but not in other regions. A peak in firn temperatures was observed at Dye-2 (located in the SW basin (66.48°N,

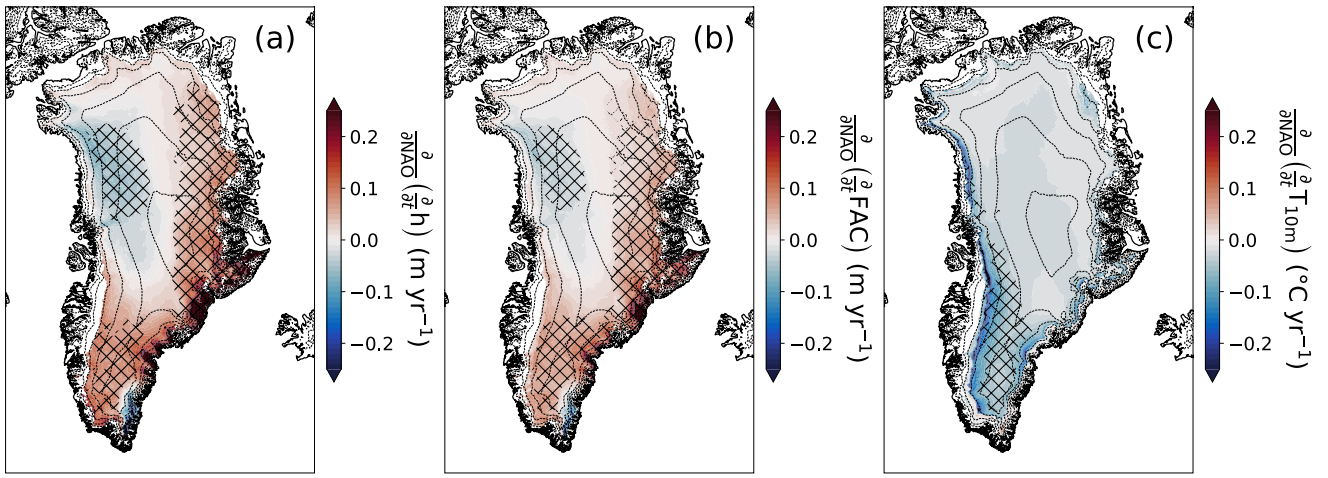

Figure 7. Sensitivity of the annual thickening or thinning rate of the firn layer (a), the rate of change of firn air content (b), and the warming or cooling rate of the firn at 10 m depth (c) to a change in the North Atlantic Oscillation (NAO) index. Sensitivities are calculated via linear regression over the period 1958–2020. Hatched areas indicate where the correlation between the rate of change and the NAO index is statistically significant ($p < 0.05$).

−46.28°E, 2130 m a.s.l.)) following the warm summer of 2012 (Vandecrux, Fausto, et al., 2020), but not at higher elevations, which is similar to our findings.

4.2. Seasonal Variability

To interpret the strongly varying amplitude of the seasonal cycle in firn thickness and FAC (Section 3.2, Figure 3a), we look at the seasonal cycle of the individual components that make up the firn thickness change: accumulation, compaction, and surface melt. The difference in seasonal amplitude is most obvious in the bordering eastern (E) and western (W) basins. Figure 8a shows the seasonal cycle in firn thickness for these two basins, averaged over 1958–2020, as well as its components. We note that there are three variables that control the seasonal amplitude of firn thickness at a specific location: (a) accumulation, (b) melt and (c) the phase lag between the accumulation on one hand and melt and compaction on the other hand. Melt and compaction rates always peak in July, when the atmospheric temperatures and downwelling radiation are at their highest. Accumulation, however, peaks in a different month depending on the location (Figure 8b).

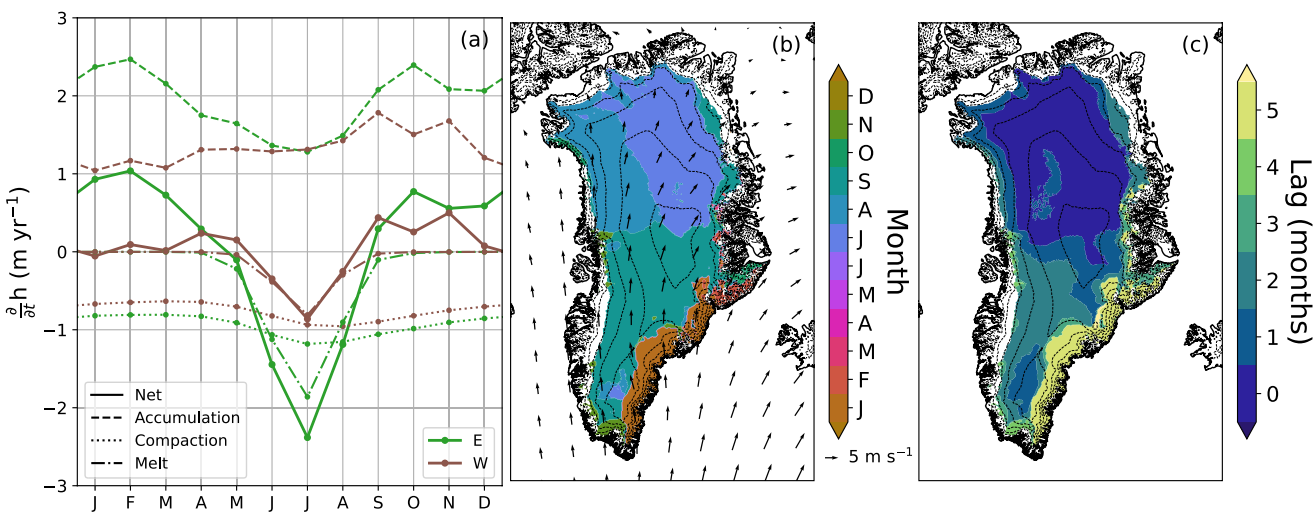

Figure 8. (a) Mean seasonal cycle of the firn thickening/thinning rate $\left(\frac{\partial}{\partial t}h\right)$ in the eastern basin (E) and in the western basin (W), respectively. (b) Month of the year with, on average, the highest accumulation for the period 1958–2020. Arrows indicate the mean 500 hPa wind during winter minus summer. (c) Absolute time lag between the firn thickening by accumulation and the thinning by compaction and melt.

Similar to our analysis of interannual variability in Section 4.1, we also look at the jet stream's influence on accumulation and temperature patterns for explaining the intra-annual variations. However, we now focus on the seasonal cycle in the jet stream rather than on longer-term changes. Generally, the polar front jet stream is weaker in summer and stronger in winter (Hall et al., 2015). As a result, the differences in the wind field at 500 hPa (arrows in Figure 8b), as well as in the accumulation rate (not shown) between winter and summer, look similar to the patterns in Figure 5 for a high and low annual NAO index. In wintertime, southeasterly winds prevail over the ice sheet, leading to a winter snowfall maximum in the east and southeast. In summer or autumn, the jet stream is weaker, which leads to a peak in snowfall in summer at most locations except the southeast. Figure 8a provides example seasonal cycles for the western (W) and eastern (E) basins. The lag between the mean thickening by accumulation and thinning by melt and compaction for the whole GrIS is shown in Figure 8c. In the western basins, most snow accumulates in the summer and autumn months, whereas in the eastern basins, most accumulation occurs in the autumn and winter months. As a result, the phase lag between accumulation and the compaction and melt in summer is maximized in the east. This leads to a larger seasonal cycle in firn thickness there. The opposite is true for most of the ice sheet's other regions, where the season of greatest accumulation and compaction rate tend to coincide. At Summit, the amount of snowfall in summer is greater than the observed change in surface height by a factor of 3 (Castellani et al., 2015). Our results suggest that the coincidence of peak accumulation with the enhanced compaction during the summer months may explain this.

5. Conclusions

Information about the thickness and density of the GrIS firn layer is required for estimates of meltwater buffering and for the conversion of ice-sheet volume to mass change. To investigate how the firn layer has changed over the past decades, we performed model simulations with the dedicated firn model IMAU-FDM v1.2G, forced by the regional climate model RACMO2.3p2 for the period 1958–2020. We find that the thickness and FAC have increased in regions above 2500 m.a.s.l., whereas it has decreased at lower elevations. This is mostly driven by an increase and, respectively, decrease in snowfall at these elevations. Consequently, the gradient of FAC with elevation has increased. Firn temperature at 10 m depth ($T_{10\mathrm{m}}$) has also been rising steadily and significantly in most regions.

We also see that, after 2012, the firn layer evolved differently compared to the two decades before. The firn thickness and air content in the southern and eastern parts of the ice sheet increased during this period. However, in the north and northwest of the ice sheet, the thickness and pore space continued to decrease. Although $T_{10\mathrm{m}}$ has been rising over the whole ice sheet for most of the simulated period, we also observe that after 2012, there has been a cooling trend in the south. Therefore, the changes in the GrIS firn are not uniform in time and space.

These temporal and spatial differences are related to changes in the large-scale atmospheric circulation, as expressed by the NAO index. Since the mid 1990s, the NAO index was mostly in a negative phase, which led to more blocking events and thus more melt, as well as less snowfall over most of the ice sheet. After 2012, however, a more positive winter NAO index led to a strong meridional gradient in the change of snow accumulation, with a snowfall increase/decrease on the eastern/western side of the ice sheet. It also led to a clear latitudinal gradient in the temperature change of the atmosphere and firn, with warming in the north and cooling in the south.

Finally, we showed that the seasonal cycle in the jet stream impacts the amplitude of the seasonal cycle in Greenland firn thickness and FAC. For most of the ice sheet, snow accumulation peaks in the summer or autumn months. This coincides with the melt season and a peak in firn compaction rates. These two processes thus partly cancel, and the resulting seasonality of the firn thickness is smaller than what would be expected when considering snowfall or melt separately. On the other hand, in the southeast of the ice sheet, snowfall peaks in winter, amplifying the seasonality in firn thickness and air content.

Our results indicate that the NAO is an important driver of GrIS firn variability on interannual and intra-annual (seasonal) time scales. The response of the ice sheet's firn layer to changes in atmospheric circulation is not spatially uniform. Therefore, care must be taken when extrapolating results from smaller to larger regions or from shorter to longer time scales. The variability of the winter NAO has been increasing recently (Hanna et al., 2022). This will likely also result in larger variability in the firn itself. However, it is uncertain whether this trend will continue. Most climate models suggest that the NAO index will increase in the future under most warming scenarios. However, GCMs generally perform poorly at simulating Greenland blocking events, and they do not

capture the observed weakening of the NAO at the beginning of the century (Delhasse et al., 2021; Hanna et al., 2018). Therefore, more research is needed to investigate the drivers of Arctic circulation patterns and how these patterns are reflected in the firn layer of the GrIS.

Data Availability Statement

All data from IMAU-FDM v1.2G and RACMO2p3.2 that have been used can be found here: https://doi.org/10.5281/zenodo.7561884. NAO Index Data provided by the Climate Analysis Section, NCAR, Boulder, USA, Hurrell et al. (2003). Updated regularly. Accessed 07 November 2022. The data can be downloaded from https://climatedataguide.ucar.edu/climate-data/hurrell-north-atlantic-oscillation-nao-index-pc-based.

Acknowledgments
This work was carried out as part of the research programme of the Netherlands Earth System Science Centre (NESSC), financially supported by the Ministry of Education, Culture and Science (OCW Grant 024.002.001). We acknowledge ECMWF for computational time on their supercomputers.

References

Bevis, M., Harig, C., Khan, S. A., Brown, A., Simons, F. J., Willis, M., et al. (2019). Accelerating changes in ice mass within Greenland, and the ice sheet's sensitivity to atmospheric forcing. *Proceedings of the National Academy of Sciences of the United States of America*, *116*(6), 1934–1939. https://doi.org/10.1073/pnas.1806562116

Brils, M., Kuipers Munneke, P., Berg, W. J. V. D., & Broeke, M. V. D. (2021). Improved representation of the contemporary Greenland ice sheet firn layer by IMAU-FDM v1. 2G. *Geoscientific Model Development*, *15*(18), 1–28. https://doi.org/10.5194/gmd-15-7121-2022

Castellani, B. B., Shupe, M. D., Hudak, D. R., & Sheppard, B. E. (2015). The annual cycle of snowfall at summit, Greenland. *Journal of Geophysical Research*, *120*(13), 6654–6668. https://doi.org/10.1002/2015JD023072

Crank, J., & Nicolson, P. (1947). A practical method for numerical evaluation of solutions of partial differential equations of the heat-conduction type. *Mathematical Proceedings of the Cambridge Philosophical Society*, *43*(1), 50–67. https://doi.org/10.1017/S0305004100023197

Cuffey, K. M., & Paterson, W. S. B. (2011). Temperature of surface layers. In *The physics of glaciers* (4th ed., Vol. 57, pp. 401–405). https://doi.org/10.3189/002214311796405906

Cullather, R. I., Andrews, L. C., Croteau, M. J., Digirolamo, N. E., Hall, D. K., Lim, Y.-K., et al. (2020). Anomalous circulation in July 2019 resulting in mass loss on the Greenland ice sheet. *Geophysical Research Letters*, *47*(17), e2020GL087263. https://doi.org/10.1029/2020GL087263

Dangendorf, S., Hay, C., Calafat, F. M., Marcos, M., Piecuch, C. G., Berk, K., & Jensen, J. (2019). Persistent acceleration in global sea-level rise since the 1960s. *Nature Climate Change*, *9*(9), 705–710. https://doi.org/10.1038/s41558-019-0531-8

Dee, D. P., Uppala, S. M., Simmons, A. J., Berrisford, P., Poli, P., Kobayashi, S., et al. (2011). The ERA-interim reanalysis: Configuration and performance of the data assimilation system. *Quarterly Journal of the Royal Meteorological Society*, *137*(656), 553–597. https://doi.org/10.1002/qj.828

De La Peña, S., Howat, I. M., Nienow, P. W., Van den Broeke, M. R., Mosley-Thompson, E., Price, S. F., et al. (2015). Changes in the firn structure of the western Greenland ice sheet caused by recent warming. *The Cryosphere*, *9*(3), 1203–1211. https://doi.org/10.5194/tc-9-1203-2015

Delhasse, A., Hanna, E., Kittel, C., & Fettweis, X. (2021). Brief communication: CMIP6 does not suggest any atmospheric blocking increase in summer over Greenland by 2100. *International Journal of Climatology*, *41*(4), 2589–2596. https://doi.org/10.1002/joc.6977

Enderlin, E. M., Howat, I. M., Jeong, S., Noh, M.-J., van Angelen, J. H., & van den Broeke, M. R. (2014). An improved mass budget for the Greenland ice sheet. *Geophysical Research Letters*, *41*(3), 866–872. https://doi.org/10.1002/2013GL059010

Ettema, J., Van den Broeke, M. R., Van Meijgaard, E., & Van de Berg, W. J. (2010). Climate of the Greenland ice sheet using a high-resolution climate model—Part 2: Near-surface climate and energy balance. *Cryosphere*, *4*(4), 529–544. https://doi.org/10.5194/tc-4-529-2010

Fettweis, X., Franco, B., Tedesco, M., van Angelen, J. H., Lenaerts, J. T. M., Van den Broeke, M. R., & Gallée, H. (2013). Estimating the Greenland ice sheet surface mass balance contribution to future sea level rise using the regional atmospheric climate model MAR. *The Cryosphere*, *7*(2), 469–489. https://doi.org/10.5194/tc-7-469-2013

Folland, C. K., Knight, J., Linderholm, H. W., Fereday, D., Ineson, S., & Hurrell, J. W. (2009). The summer North Atlantic oscillation: Past, present, and future. *Journal of Climate*, *22*(5), 1082–1103. https://doi.org/10.1175/2008JCLI2459.1

Forster, R. R., Box, J. E., van den Broeke, M. R., Miège, C., Burgess, E. W., van Angelen, J. H., et al. (2014). Extensive liquid meltwater storage in firn within the Greenland ice sheet. *Nature Geoscience*, *7*(2), 95–98. https://doi.org/10.1038/ngeo2043

Hall, R., Erdélyi, R., Hanna, E., Jones, J. M., & Scaife, A. A. (2015). Drivers of North Atlantic polar front jet stream variability. *International Journal of Climatology*, *35*(8), 1697–1720. https://doi.org/10.1002/joc.4121

Hanna, E., Cappelen, J., Fettweis, X., Mernild, S. H., Mote, T. L., Mottram, R., et al. (2021). Greenland surface air temperature changes from 1981 to 2019 and implications for ice-sheet melt and mass-balance change. *International Journal of Climatology*, *41*(S1), E1336–E1352. https://doi.org/10.1002/joc.6771

Hanna, E., Cropper, T. E., Hall, R. J., Cornes, R. C., & Barriendos, M. (2022). Extended North Atlantic oscillation and Greenland blocking indices 1800–2020 from new meteorological reanalysis. *Atmosphere*, *13*(3), 436. https://doi.org/10.3390/atmos13030436

Hanna, E., Cropper, T. E., Jones, P. D., Scaife, A. A., & Allan, R. (2015). Recent seasonal asymmetric changes in the NAO (a marked summer decline and increased winter variability) and associated changes in the AO and Greenland blocking index. *International Journal of Climatology*, *35*(9), 2540–2554. https://doi.org/10.1002/joc.4157

Hanna, E., Fettweis, X., & Hall, R. J. (2018). Recent changes in summer Greenland blocking captured by none of the CMIP5 models. *The Cryosphere Discussions*, 1–8.

Hanna, E., Huybrechts, P., Cappelen, J., Steffen, K., Bales, R. C., Burgess, E., et al. (2011). Greenland ice sheet surface mass balance 1870 to 2010 based on Twentieth Century reanalysis, and links with global climate forcing. *Journal of Geophysical Research*, *116*(D24), D24121. https://doi.org/10.1029/2011JD016387

Hanna, E., Jones, J. M., Cappelen, J., Mernild, S. H., Wood, L., Steffen, K., & Huybrechts, P. (2013). The influence of North Atlantic atmospheric and oceanic forcing effects on 1900–2010 Greenland summer climate and ice melt/runoff. *International Journal of Climatology*, *33*(4), 862–880. https://doi.org/10.1002/joc.3475

Hawley, R. L., Neumann, T. A., Stevens, C. M., Brunt, K. M., & Sutterley, T. C. (2020). Greenland ice sheet elevation change: Direct observation of process and attribution at summit. *Geophysical Research Letters*, *47*(22), 1–8. https://doi.org/10.1029/2020GL088864

Heilig, A., Eisen, O., MacFerrin, M., Tedesco, M., & Fettweis, X. (2018). Seasonal monitoring of melt and accumulation within the deep percolation zone of the Greenland Ice Sheet and comparison with simulations of regional climate modeling. *The Cryosphere*, *12*(6), 1851–1866. https://doi.org/10.5194/tc-12-1851-2018

Herron, M. M., & Langway, C. C. (1980). Firn densification: An empirical model. *Journal of Glaciology*, *25*(93), 373–385. https://doi.org/10.1017/S0022143000015239

Hersbach, H., Bell, B., Berrisford, P., Hirahara, S., Horányi, A., Muñoz-Sabater, J., et al. (2020). The ERA5 global reanalysis. *Quarterly Journal of the Royal Meteorological Society*, *146*(730), 1999–2049. https://doi.org/10.1002/qj.3803

Huai, B., van den Broeke, M. R., & Reijmer, C. H. (2020). Long-term surface energy balance of the western Greenland Ice Sheet and the role of large-scale circulation variability. *The Cryosphere*, *14*(11), 4181–4199. https://doi.org/10.5194/tc-14-4181-2020

Hurrell, J. W., & Deser, C. (2009). North Atlantic climate variability: The role of the North Atlantic oscillation. *Journal of Marine Systems*, *78*(1), 28–41. https://doi.org/10.1016/j.jmarsys.2008.11.026

Hurrell, J. W., Kushnir, Y., Ottersen, G., & Visbeck, M. (2003). An overview of the North Atlantic oscillation. In *The North Atlantic oscillation: Climatic significance and environmental impact* (pp. 1–35). American Geophysical Union (AGU). https://doi.org/10.1029/134GM01

Jun, L., & Zwally, H. J. (2002). Modeled seasonal variations of firn density induced by steady-state surface air-temperature cycle. *Annals of Glaciology*, *34*, 299–302. https://doi.org/10.3189/172756402781817707

Khan, S. A., Bamber, J. L., Rignot, E., Helm, V., Aschwanden, A., Holland, D. M., et al. (2022). Greenland mass trends from airborne and satellite altimetry during 2011–2020. *Journal of Geophysical Research: Earth Surface*, *127*(4), e2021JF006505. https://doi.org/10.1029/2021JF006505

Kuipers Munneke, P., Ligtenberg, S. R. M., Noël, B. P. Y., Howat, I. M., Box, J. E., Mosley-Thompson, E., et al. (2015). Elevation change of the Greenland ice sheet due to surface mass balance and firn processes, 1960–2014. *The Cryosphere*, *9*(6), 2009–2025. https://doi.org/10.5194/tc-9-2009-2015

Kuipers Munneke, P., van den Broeke, M. R., Lenaerts, J. T. M., Flanner, M. G., Gardner, A. S., & van de Berg, W. J. (2011). A new albedo parameterization for use in climate models over the Antarctic ice sheet. *Journal of Geophysical Research*, *116*(D5), D05114. https://doi.org/10.1029/2010JD015113

Lenaerts, J. T. M., Smeets, C. J. P. P., Nishimura, K., Eijkelboom, M., Boot, W., Van den Broeke, M. R., & Van de Berg, W. J. (2014). Drifting snow measurements on the Greenland Ice Sheet and their application for model evaluation. *The Cryosphere*, *8*(2), 801–814. https://doi.org/10.5194/tc-8-801-2014

Ligtenberg, S. R. M., Helsen, M. M., & Van den Broeke, M. R. (2011). An improved semi-empirical model for the densification of Antarctic firn. *The Cryosphere*, *5*(4), 809–819. https://doi.org/10.5194/tc-5-809-2011

McGrath, D., Colgan, W., Bayou, N., Muto, A., & Steffen, K. (2013). Recent warming at Summit, Greenland: Global context and implications. *Geophysical Research Letters*, *40*(10), 2091–2096. https://doi.org/10.1002/grl.50456

McLeod, J. T., & Mote, T. L. (2016). Linking interannual variability in extreme Greenland blocking episodes to the recent increase in summer melting across the Greenland ice sheet. *International Journal of Climatology*, *36*(3), 1484–1499. https://doi.org/10.1002/joc.4440

McMillan, M., Leeson, A., Shepherd, A., Briggs, K., Armitage, T. W. K., Hogg, A., et al. (2016). A high-resolution record of Greenland mass balance. *Geophysical Research Letters*, *43*(13), 7002–7010. https://doi.org/10.1002/2016GL069666

Mouginot, J., Rignot, E., Bjørk, A. A., van den Broeke, M., Millan, R., Morlighem, M., et al. (2019). Forty-six years of Greenland ice sheet mass balance from 1972 to 2018. *Proceedings of the National Academy of Sciences of the United States of America*, *116*(19), 9239–9244. https://doi.org/10.1073/pnas.1904242116

Nghiem, S. V., Hall, D. K., Mote, T. L., Tedesco, M., Albert, M. R., Keegan, K., et al. (2012). The extreme melt across the Greenland ice sheet in 2012. *Geophysical Research Letters*, *39*(20), 6–11. https://doi.org/10.1029/2012GL053611

Noël, B., van de Berg, W. J., van Wessem, J. M., van Meijgaard, E., van As, D., Lenaerts, J. T. M., et al. (2018). Modelling the climate and surface mass balance of polar ice sheets using RACMO2—Part 1: Greenland (1958–2016). *The Cryosphere*, *12*(3), 811–831. https://doi.org/10.5194/tc-12-811-2018

Noël, B., Van de Berg, W. J., Lhermitte, S., Wouters, B., Machguth, H., Howat, I., et al. (2017). A tipping point in refreezing accelerates mass loss of Greenland's glaciers and ice caps. *Nature Communications*, *8*(1), 14730. https://doi.org/10.1038/ncomms14730

Noël, B., van Kampenhout, L., Lenaerts, J. T. M., van de Berg, W. J., & van den Broeke, M. R. (2021). A 21st century warming threshold for sustained Greenland ice sheet mass loss. *Geophysical Research Letters*, *48*(5), 1–9. https://doi.org/10.1029/2020GL090471

Orsi, A. J., Kawamura, K., Masson-Delmotte, V., Fettweis, X., Box, J. E., Dahl-Jensen, D., et al. (2017). The recent warming trend in North Greenland. *Geophysical Research Letters*, *44*(12), 6235–6243. https://doi.org/10.1002/2016GL072212

Polashenski, C., Courville, Z., Benson, C., Wagner, A., Chen, J., Wong, G., et al. (2014). Observations of pronounced Greenland ice sheet firn warming and implications for runoff production. *Geophysical Research Letters*, *41*(12), 4238–4246. https://doi.org/10.1002/2014GL059806

Ramos Buarque, S., & Salas y Melia, D. (2018). Link between the North Atlantic oscillation and the surface mass balance components of the Greenland ice sheet under preindustrial and last interglacial climates: A study with a coupled global circulation model. *Climate of the Past*, *14*(11), 1707–1725. https://doi.org/10.5194/cp-14-1707-2018

Rennermalm, Å. K., Hock, R., Covi, F., Xiao, J., Corti, G., Kingslake, J., et al. (2022). Shallow firn cores 1989-2019 in southwest Greenland's percolation zone reveal decreasing density and ice layer thickness after 2012. *Journal of Glaciology*, *68*(269), 431–442. https://doi.org/10.1017/jog.2021.102

Sandberg Sørensen, L., Simonsen, S. B., Forsberg, R., Khvorostovsky, K., Meister, R., & Engdahl, M. E. (2018). 25 years of elevation changes of the Greenland Ice Sheet from ERS, Envisat, and CryoSat-2 radar altimetry. *Earth and Planetary Science Letters*, *495*, 234–241. https://doi.org/10.1016/j.epsl.2018.05.015

Shepherd, A., Ivins, E., Rignot, E., Smith, B., van den Broeke, M., Velicogna, I., et al. (2020). Mass balance of the Greenland ice sheet from 1992 to 2018. *Nature*, *579*(7798), 233–239. https://doi.org/10.1038/s41586-019-1855-2

Steffen, K., & Box, J. (2001). Surface climatology of the Greenland ice sheet: Greenland climate network 1995–1999. *Journal of Geophysical Research*, *106*(D24), 33951–33964. https://doi.org/10.1029/2001JD900161

Stevens, C. M., Verjans, V., Lundin, J. M. D., Kahle, E. C., Horlings, A. N., Horlings, B. I., & Waddington, E. D. (2020). The community firn model (CFM) v1.0. *Geoscientific Model Development*, *13*(9), 4355–4377. https://doi.org/10.5194/gmd-13-4355-2020

Tedesco, M., & Fettweis, X. (2020). Unprecedented atmospheric conditions (1948-2019) drive the 2019 exceptional melting season over the Greenland ice sheet. *The Cryosphere*, *14*(4), 1209–1223. https://doi.org/10.5194/tc-14-1209-2020

Uppala, S. M., Kållberg, P. W., Simmons, A. J., Andrae, U., Bechtold, V. D. C., Fiorino, M., et al. (2005). The ERA-40 re-analysis. *Quarterly Journal of the Royal Meteorological Society*, *131*(612), 2961–3012. https://doi.org/10.1256/qj.04.176

van Angelen, J. H., Van den Broeke, M. R., Wouters, B., & Lenaerts, J. T. M. (2014). Contemporary (1960–2012) evolution of the climate and surface mass balance of the Greenland ice sheet. *Surveys in Geophysics*, *35*(5), 1155–1174. https://doi.org/10.1007/s10712-013-9261-z

Vandecrux, B., Fausto, R. S., van As, D., Colgan, W., Langen, P. L., Haubner, K., et al. (2020). Firn cold content evolution at nine sites on the Greenland ice sheet between 1998 and 2017. *Journal of Glaciology*, *66*(258), 1–12. https://doi.org/10.1017/jog.2020.30

Vandecrux, B., Mottram, R., Langen, L., Fausto, P. S., Olesen, M., Max Stevens, C., et al. (2020). The firn meltwater Retention Model Intercomparison Project (RetMIP): Evaluation of nine firn models at four weather station sites on the Greenland ice sheet. *The Cryosphere*, *14*(11), 3785–3810. https://doi.org/10.5194/tc-14-3785-2020

Van den Broeke, M. R., Enderlin, E. M., Howat, I. M., Kuipers Munneke, P., Noël, B. P. Y., Jan Van De Berg, W., et al. (2016). On the recent contribution of the Greenland ice sheet to sea level change. *The Cryosphere*, *10*(5), 1933–1946. https://doi.org/10.5194/tc-10-1933-2016

Wang, W., Zender, C. S., & van As, D. (2018). Temporal characteristics of cloud radiative effects on the Greenland ice sheet: Discoveries from multiyear automatic weather station measurements. *Journal of Geophysical Research: Atmospheres*, *123*(20), 11348–11361. https://doi.org/10.1029/2018JD028540

Wang, W., Zender, C. S., van As, D., & Miller, N. B. (2019). Spatial distribution of melt season cloud radiative effects over Greenland: Evaluating satellite observations, reanalyzes, and model simulations against in situ measurements. *Journal of Geophysical Research: Atmospheres*, *124*(1), 57–71. https://doi.org/10.1029/2018JD028919

Zhang, B., Liu, L., Khan, S. A., van Dam, T., Bjørk, A. A., Peings, Y., et al. (2019). Geodetic and model data reveal different spatio-temporal patterns of transient mass changes over Greenland from 2007 to 2017. *Earth and Planetary Science Letters*, *515*, 154–163. https://doi.org/10.1016/j.epsl.2019.03.028

Zwally, H. J., & Jun, L. (2002). Seasonal and interannual variations of firn densification and ice-sheet surface elevation at the Greenland summit. *Journal of Glaciology*, *48*(161), 199–207. https://doi.org/10.3189/172756502781831403